International Journal of Pharmaceutics 524 (2017) 330–338

Contents lists available at ScienceDirect

International Journal of Pharmaceutics

journal homepage: www.elsevier.com/locate/ijpharm

Computational and experimental approaches for development of methotrexate nanosuspensions by bottom-up nanoprecipitation

Aline Martins dos Santos[a,*], Flávia Chiva Carvalho[b], Deiver Alessandro Teixeira[c], David Lima Azevedo[d], Wander Miguel de Barros[c], Maria Palmira Daflon Gremião[a,*]

[a] Department of Drugs and Pharmaceutics, Faculty of Pharmaceutical Sciences, São Paulo State University-UNESP, SP, 14801-902, Brazil
[b] Faculty of Pharmaceutical Sciences, Federal University of Alfenas-UNIFAL, MG, 37130-000, Brazil
[c] Federal Institute of Mato Grosso-IFMT, MT, 78050-560, Brazil
[d] Institute of Physical—University of Brasília-UnB, DF, 70919-970, Brazil

ARTICLE INFO

Article history:
Received 15 July 2016
Received in revised form 21 March 2017
Accepted 26 March 2017
Available online 28 March 2017

Keywords:
Nanosuspensions
Bottom-up process
Acid-base neutralization
Methotrexate
Computational modeling

ABSTRACT

Development of nanosuspensions offers a promising tool for formulations involving poorly water-soluble drugs. In this study, methotrexate (MTX) nanosuspensions were prepared using a bottom-up process based on acid-base neutralization reactions. Computational studies were performed to determine structural and electronic properties for isolated molecules and molecular clusters in order to evaluate the mechanism of MTX nanoparticle formation. Computational results indicated that the clusters in zwitterionic and cationic states presented larger dimensions and higher energies of interaction between MTX molecules, which favored aggregation. In contrast, the clusters in the anionic state exhibited lower energies of interaction, indicating aggregation was less likely to occur. Experimental results indicated that the higher the HCl proportion during drug precipitation, the greater the particle size, resulting in micrometric particles (2874–7308 nm) (cationic and zwitterionic forms). However, MTX nanoparticles ranging in size from 132 to 186 nm were formed using the lowest HCl proportion during drug precipitation (anionic form). In vitro release profiles indicated that the drug release rate from nanosuspension was increased (approximately 2.6 times) over that of the raw material. Overall, computational modeling and experimental analysis were complementary and assisted in the rational design of the nanosuspension based on acid-base reactions.

1. Introduction

Nanosuspensions are a relatively new trend in pharmaceutical technology because of the benefits of reducing the size of insoluble drug particles. Nano-ranged particles can lead to an increase in the dissolution rate and bioavailability of a drug, especially one with stability and solubility problems (Bose et al., 2012; George and Ghosh, 2013; Möschwitzer, 2013; Sinha et al., 2013). Additionally, particle size reduction can increase penetration through biological barriers and cell membranes, which can lead to an improved drug residence time in a specific tissue or organ (Alaei et al., 2016; Collnot et al., 2012; Rabinow, 2004). Additional advantages include dose and toxicity reduction, increased drug concentration in affected tissues or organs, and better adhesion of nanoparticles to mucosal surfaces (Das and Suresh, 2011; Jacobs and Müller, 2002; Tian et al., 2013). In addition, nanosuspensions can be administered by various routes, including oral (Xu et al., 2012), parenteral (Tian et al., 2013), nasal (Bhavna et al., 2014), ophthalmic (Pignatello et al., 2002), and pulmonary (Jacobs and Müller, 2002).

Nanosuspensions are submicron colloidal dispersions of pure drug particles, which are stabilized by surfactants, polymers, or a combination of both (Rabinow, 2004). A reduction in particle size leads to an increase in dissolution rate because of an increased surface area, according to the Noyes-Whitney equation (Noyes and Whitney, 1897), and an enhancement in saturation solubility of the drug, based on the Ostwald-Freundlich equation (Sinha et al., 2013; Xu et al., 2012).

Nanosuspensions can be prepared using top-down processes, which involve drug particle size reduction using various techniques, including media milling, microfluidization and high-pressure homogenization. The wet milling and high-pressure homogenization methods are widely exploited because they efficiently produce

* Corresponding authors.
E-mail addresses: asantos@fcfar.unesp.br, aline.martinsdossantos@yahoo.com.br (A.M. dos Santos), pgremiao@fcfar.unesp.br (M.P.D. Gremião).

http://dx.doi.org/10.1016/j.ijpharm.2017.03.068
0378-5173/

small particles and do not require organic solvents, making them more feasible for industry production. However, these techniques involve a high energy input, which generate heat, making it difficult to process thermolabile materials. In addition, the large amount of energy can produce amorphous particles and cause deformation of crystals (Chen et al., 2008; Rabinow, 2004; Sinha et al., 2013; Verma et al., 2009).

Another technique for making nanosuspensions is the bottom-up process, also known as the precipitation process, in which the particles are formed from a molecular state, based on the precipitation of particles from a supersaturated drug solution. The drug can be precipitated using methods such as solvent evaporation, supercritical fluid, antisolvent precipitation and chemical precipitation. For drugs with pH-dependent solubility, precipitation can be accomplished utilizing acid-base neutralization reactions. The bottom-up method requires a low energy input, making it useful for thermolabile materials, and is also simple and inexpensive (Chen et al., 2008; Mou et al., 2011; Verma et al., 2009).

Methotrexate (MTX) ((2S)-2-[[2,4-diaminopteridin-6-yl)methyl-methylamino]benzoyl]amino]pentanedioic acid) is a chemotherapeutic drug that, acts as a folic acid antagonist and interferes with the formation of DNA, RNA, and proteins. The aqueous solubility of MTX is pH-dependent ranging from 0.9 mM (pH 5) to 20 mM (pH 7). It has a log P of −1.85 (Chen et al., 2012; Hansch et al., 1995; Rubino, 2001).

It is widely used in the treatment of various diseases, including leukemia, osteosarcoma, non-Hodgkin's lymphoma, head and neck cancer, lung cancer, breast cancer, colorectal cancer, choriocarcinoma, as well as autoimmune diseases such as psoriasis and rheumatoid arthritis. However, MTX is poorly water-soluble and has a bioavailability limited by its poor solubility and slow dissolution rate. It also is associated with several side effects when administered at high doses (Chen et al., 2012; Pereira et al., 2014; Rubino, 2001).

The development of nanosuspensions represents a promising strategy for drugs such as MTX that have poor water-solubility. This study aimed to develop nanosuspensions using a bottom-up technique because MTX exhibits a pH-dependent solubility and particles of MTX can be formed using acid-base neutralization. The effect of variables, such as the different acid and base proportions employed in the MTX solubilization and precipitation, were evaluated regarding particle formation and size. The parameters investigated were size, polydispersity index (PDI), zeta potential, Fourier transform infrared spectroscopy (FTIR), drug content, and *in vitro* particle dissolution rate.

Computational modeling studies, especially quantum chemistry calculations, can be used in pharmaceutical nanotechnology together with experimental studies to advance the understanding of the formation, mechanism of action, interaction, mechanical properties, characterization, and stability of drug delivery systems (Bunker et al., 2016; De Souza et al., 2016; Ramezanpour et al., 2016). In this study, the interaction energies of the particles were evaluated with computational calculations (quantum chemistry calculations) using density functional theory (DFT) to obtain various properties, including the equilibrium geometry for each molecular system, Mulliken charges, orbital energies, and molecular orbitals. Computational modeling and experimental analysis were combined synergistically for the rational design of MTX nanosuspensions and to understand the experimental methods.

2. Materials and methods

2.1. Computational study

Quantum chemistry calculations were performed using DFT as implemented in the GAUSSIAN 09W package (Frisch et al., 2009) because of their sufficient accuracy and lower computational cost when compared to *ab initio* Hartree-Fock, as observed in other studies (Becke, 1988; Dennington et al., 2009; Frisch et al., 2009; Lewars, 2003; Rassolov et al., 2001). Generalized gradient approximation (GGA) was used with the B3LYP (Becke, 1988) exchange correlation functional, along with the 6-31G(d,p) basis set (Rassolov et al., 2001). This basis functions were chosen due of its additional polarization and diffuse functions that have advantage to describe better equilibrium geometry, ground state energies, charges, and electronic densities for second and third row atoms.

In this study, it was used DFT with an implicit water solvation PCM model (Tomasi et al., 2005). The PCM (Polarizable Continuum Model) calculates the free energy of solvation by attempting to sum over three different terms (Eq. (1)):

$$G_{solvatation} = G_{electrostatic} + G_{\text{dispersion}-\text{repulsion}} + G_{\text{cavitation}} \quad (1)$$

The cavity used in the PCM is generated by a series of overlapping spheres normally defined by the van der Waals radii of the individual atoms (Fig. 1). It is possible in Gaussian to customize the spherical radii.

The mathematical formalism for the integral equation formalism PCM (IEF-PCM) model (this is the model that was employed by Gaussian) is presented below. The complete Hamiltonian of the solute molecule can be written as (Eq. (2)):

$$H = H^0 + V_{MS} + V'(t) \quad (2)$$

Where H^0 is the Hamiltonian in vacuo, V_{MS} is the solute-solvent molecule interaction, and the V'(t) component is the time-dependent perturbation on the solute molecule. The V_{MS} component is further defined as (Eq. (3)):

$$V_{MS} = \int_{\Sigma} V(s)\left[\sigma^N(s) + \sigma^e(s)(\rho;s)\right]ds \quad (3)$$

Here, the surface charge density is broken into two parts for the nuclei ($\sigma^N(s)$) and the electrons ($\sigma^e(\rho;s)$) for the solute. The V(s) component is the electrostatic potential of the solute molecule calculated on the cavity surface, Σ. The last element to the

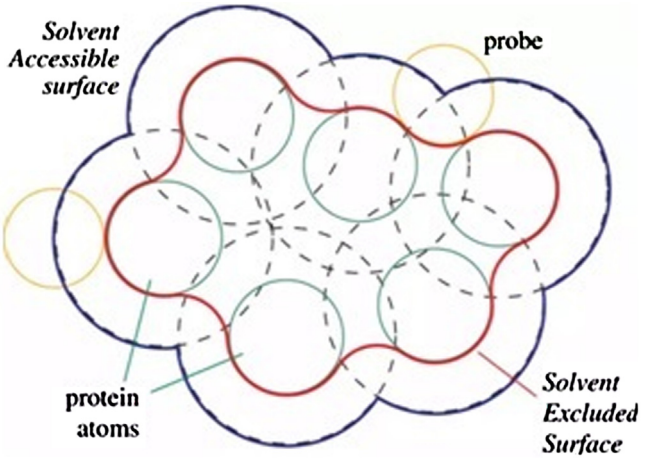

Fig. 1. Illustration of cavity of solute-solvent interaction. Solvent accessible surface (SAS) traced out by the center of the probe representing a solvent molecule (blue line). The solvent excluded surface (SES) is the topological boundary of the union of all possible probes that do not overlay with the molecule (red line). (For interpretation of the references to color in this figure legend, the reader is referred to the web version of this article.)

Hamiltonian of the solute molecule is (Eq. (4)):

$$V'(t) = -\frac{1}{2}(\mu_{el}^{e})_{\alpha}E_{\alpha}^{\omega}(e^{i\omega t} + e^{-i\omega t}) - \frac{1}{2}\int_{\Sigma} V(s)\frac{\partial\sigma_{\omega}^{ex}}{\partial E_{\alpha}^{\omega}}E_{\alpha}^{\omega}(e^{i\omega t} + e^{-i\omega t})ds \quad (4)$$

This term describes the cavity-field effect and the response of the solvent to the external field after creation of the solute cavity in the solvent. This allows for the direct calculation of the effective polarizabilities of the molecule in the solvent. The free energy of solvation for any PCM calculation is primarily the electrostatic energy.

The polar medium could provide the needed environment for zwitterion stabilization, and the final equilibrium geometry obtained is correspondent to a real zwitterion structure. Thus, this test allowed the determination of several properties, including the equilibrium geometry for each molecular system, populational Mulliken analysis, orbital energies, and molecular orbitals.

The Adsorption Locator module of the Materials Studio suite software (Anon., 2017; Rappe et al., 1993, 1992) was used to find the lowest energy cluster for different molecular quantities. The adsorption cluster was obtained by increasing the number of molecules gradually until the number was reached for each type of cluster. We performed a simulated annealing using the universal force field (UFF), where the criteria used for adsorption simulation were five cycles with 15000 Monte Carlo steps using the default probabilities for rotate, translate and regrow. The convergence optimization criteria were an energy or force change less than or equal to 10^{-3} kcal/mol or 0.5 kcal/mol Å^{-1}, respectively, between successive steps. From the ten energy configurations, the most energetically favorable (the lowest energy configuration), was chosen and this protocol was systematically used for each type of cluster. The interaction energy of the MTX molecules ($E_{inttotal}$) was obtained by difference between the cluster energy for each state ($E_{cluster}$) and the individual energy of the species (anionic, zwitterionic and cationic) (E_{specie}) of the total molecules in the analyzed state, according to the following equation (Eq. (5)):

$$E_{int\ total} = E_{cluster} - \sum E_{specie} \quad (5)$$

The GaussView package (Dennington et al., 2009) was used to generate and visualize all the figures of the computational calculations. In order to visualize the figures for this study, spheres of different sizes, symbols, and colors were used for each chemical element, as shown in Fig. 2a.

2.2. Experimental study

2.2.1. Materials

MTX was purchased from Fagron Pharmaceutical (São Paulo, Brazil), sodium hydroxide was provided by Grupo Química (Rio de Janeiro, Brazil), 37% hydrochloric acid was supplied by Quimis (São Paulo, Brazil), and purified water (Milli Q Millipore).

2.2.2. Preparation of MTX nanosuspensions by bottom-up process

MTX (25 mg/mL) was solubilized in water (20 mL), and the pH was adjusted with two different volumes of 1 mol/L NaOH (Table 1), under magnetic stirring, in order to obtain 1:1 and 2:1 molar proportions of the drug. These proportions guaranteed an interaction with one and two carboxylic groups of MTX, respectively, in addition to its solubilization.

To precipitate MTX particles, different volumes of 1 mol/L HCl were added dropwise to the drug solution while stirring using an Ultra Turrax (Turratec TE-102, Tecnal, Brazil) under ice bath, at 24000 rpm for 5 min. The volumes and molar ratios used are indicated in Table 1. The abbreviation F was used to identify formulations as follows: F1, F2, F3, F4, F5, F6, F7, and F8.

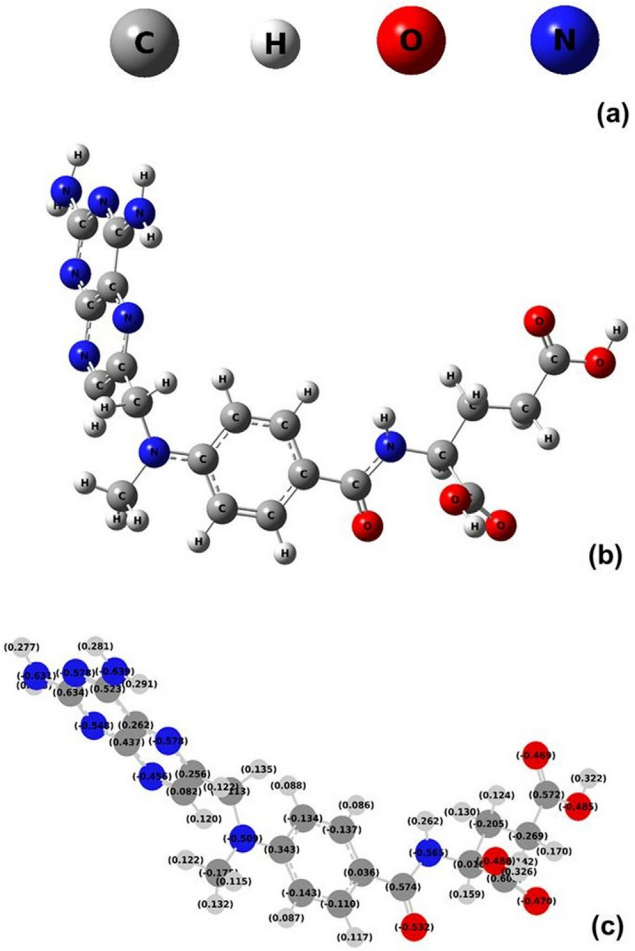

Fig. 2. Representation of each chemical element in the surface molecular structures (a). The geometry of the methotrexate (MTX) (b) compound in a minimum energy state; (c) regions of high reactivity, observed from the Mulliken charges obtained for each atom.

2.2.3. Physicochemical characterization of MTX nanosuspensions

2.2.3.1. Particle size and PDI determination. The particle size and PDI of MTX nanosuspensions were determined by dynamic light scattering using a Zetasizer Nanoseries (Malvern Instruments, Worcestershire, UK). Before measurement, the nanosuspensions were diluted (1:9; v/v) in Milli-Q water, which was the vehicle of the nanosuspension, and the final pH of each nanosuspension were maintained. All measurements were performed at 25 °C in

Table 1
Composition of the formulations (F): molar ratios of solubilizing agent (NaOH 1 mol/L) and precipitation agent (HCl 1 mol/L) used for preparing the samples using the bottom-up method.

Formulation	Molar ratio MTX:NaOH:HCl
F1	1:1:0.5
F2	1:2:1
F3	1:1:1.3
F4	1:1:1.4
F5	1:1:1.7
F6	1:2:1.9
F7	1:2:2.2
F8	1:2:3

triplicate and the mean values and standard deviations were reported.

2.2.3.2. Zeta potential measurement. Zeta potential was determined by measuring particle mobility under an applied electric field using a Zetasizer Nanoseries (Malvern Instruments, Worcestershire, UK). Prior to the measurement, samples were diluted (1:9; v/v) in Milli-Q water. All measurements were performed at 25 °C in triplicate and the mean values and standard deviations were reported.

2.2.3.3. FTIR. The FTIR absorption spectra of the nanosuspensions and the raw drug were recorded on a Thermo Scientific Nicolet 155 spectrophotometer (Thermo Fisher Scientific, Pittsburgh, PA, USA) at frequencies ranging from 400 to 4000 cm^{-1} with a 2 cm^{-1} resolution. Samples were frozen at −80 °C for 12 h and then lyophilized by Thermo Micromodulyo-115 (Thermo Fisher Scientific, Asheville, NC, USA) for 24 h. Thereafter, the samples and raw drug were each mixed with potassium bromide and pressed into pellets before testing. F2, F3 and F7 were selected for FTIR studies to represent the different molecular forms of MTX (anionic, zwitterionic and cationic).

2.2.3.4. ATR-FTIR. The ATR-FTIR spectra of the liquid form nanosuspensions (F2, F3, and F7) and the raw drug were measured using a Vertex 70 spectrophotometer (Bruker, UK) fitted with a diamond ATR crystal. The spectra were recorded across the range of 400 to 4000 cm^{-1}, using a spectral resolution of 4 cm^{-1} and 64 scans.

2.2.3.5. Drug content study. The MTX nanosuspensions were centrifuged (centrifuge Labnet, model Spectrafuge 16 M, Edison, NJ, USA) at 14000 rpm, at 25 °C for 15 min and the supernatants were filtered through 0.45-μm membrane filters. The amount of MTX in each sample was determined using a UV spectrophotometer (Hewlett Packard-Kayak XA, USA) at 303 nm. The analysis was performed in triplicate, and the drug content was calculated by the following equation (Eq. (6)):

$$\text{Drug content } (\%) = \left(\frac{\text{Theoretical drug content} - \text{Supernatant drug content}}{\text{Theoretical drug content}}\right) \times 100 \quad (6)$$

2.2.3.6. In vitro dissolution study. The dissolution tests were performed on a Hanson Research (New Hanson SR-8 Plus, Chastworth, USA) dissolution station, using a USP apparatus II (paddle) (USP, 2007) at 50 rpm and 37 ± 0.4 °C. Five milliliters of each sample, equivalent to 125 mg MTX, was added to 900 mL of phosphate buffer solution (pH 6.8). Aliquots were withdrawn at predetermined times and immediately replaced with an equivalent amount of fresh dissolution media to maintain the sink condition. Samples were filtered through a 0.45-μm cellulose acetate membrane filter before analysis. The concentration of MTX released from each sample was determined using a UV spectrophotometer (Hewlett Packard-Kayak) at 303 nm. Dissolution studies were performed in triplicate.

3. Results and discussion

3.1. Computational study: a tool for the development of nanosuspensions

Quantum chemistry methods and molecular modeling techniques allow for the investigation of a variety of molecular properties, such as reactivity, disposition, and chemical bonding, as well as the evaluation of molecular fragments and substituents. Atomic charge is an important parameter that can be determined using the Mulliken charges method (Gece, 2008). This numerical quantity provided a qualitative understanding of the molecular structure with respect to the reactivity of the molecule and the atomic charge described the polarity of the molecule.

Computational modeling studies were used to evaluate the behavior of the MTX molecule in three different states (anionic,

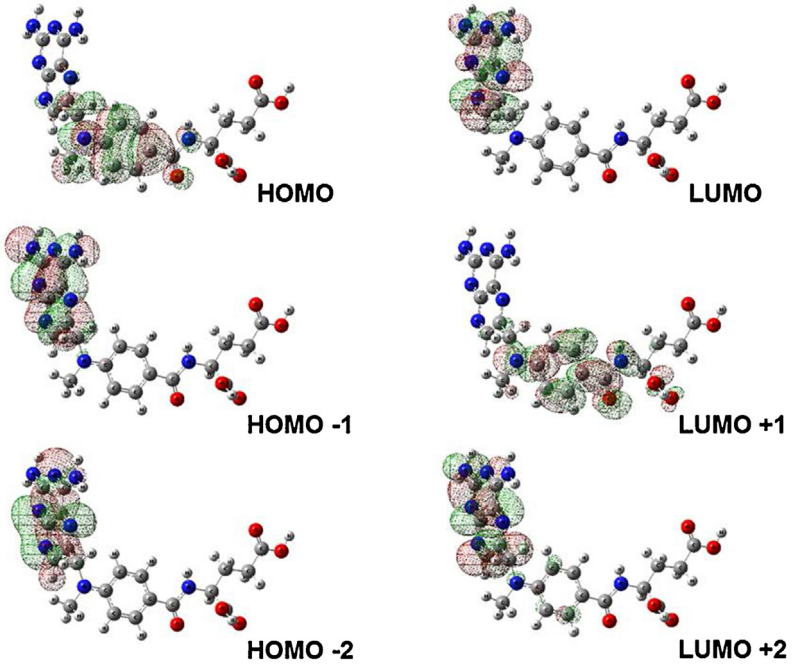

Fig. 3. The spatial distribution of the frontier molecular orbitals of methotrexate (MTX): the highest occupied molecular orbital (HOMO) and the lowest unoccupied molecular orbital (LUMO).

zwitterionic, and cationic). This provided a mechanism for understanding the experimental results from this study.

The geometry of the MTX compound revealed a minimum energy state (Fig. 2b) and exhibited a considerable electronic density owing to the presence of different functional groups as amine, amide, carboxylic acids, and benzene ring. These groups represented three different regions in the molecule; (i) pteridine terminal group, (ii) carboxylic acid terminal groups and (iii) amine and amide aromatic centered groups. The presence of these groups provide electronic density along the whole molecule.

The populational analysis of Mulliken allowed observing regions of some atoms, sites with high or low electronic density (Fig. 2c). Thus, it was observed that the electronic density is higher over the nitrogen atoms, due to the negative value of the Mulliken charges, associated to the effect of common resonance to hexenes cycle. In the region of the carboxylic acid terminal group, was observed a more positive value of the acid hydrogen bonded to the carboxylic acid group next to the amide group, indicating the more acidic hydrogen. Besides, the oxygen of the amide group presented a high negative value. The association of the acid hydrogen closed to the amide oxygen provides a more reactive region.

Molecular frontier orbital were used to evaluate the regions of the molecule that are acceptors or donors of electrons. These regions are the reactive regions of the molecule (Li et al., 2014; Macedo et al., 2012). The HOMO (highest occupied molecular orbital) can donate electrons because its orbital is more external (high energy) than the other occupied orbitals, whereas the LUMO (lowest unoccupied molecular orbital) can accept electrons because it is lower energy than the other unoccupied orbitals. Molecular orbitals are denominated with reference either to HOMO or LUMO orbital, i.e., the label HOMO-*n* stands for *n*th orbital below the HOMO, whereas the LUMO+*m* stands for *m*th orbital above the LUMO (Kokalj and Peljhan, 2010).

From the results of the quantum chemistry calculations, the frontiers orbital, largely used to understand the reactivity and transport properties of molecules, were identified. In Fig. 3, the HOMO orbital was observed to be localized over the benzene rings; this was the region that was favorable for the donation or sharing of electrons. The HOMO -1 and HOMO -2 were localized over nitrogen atoms and indicated regions of greater reactivity. The LUMO orbital and LUMO +2 were localized over the same region as HOMO -1 and HOMO -2; this indicated a highly localized frontier orbitals molecule and indicated the region most favorable for reactivity (donor/acceptor) or interaction with other molecules.

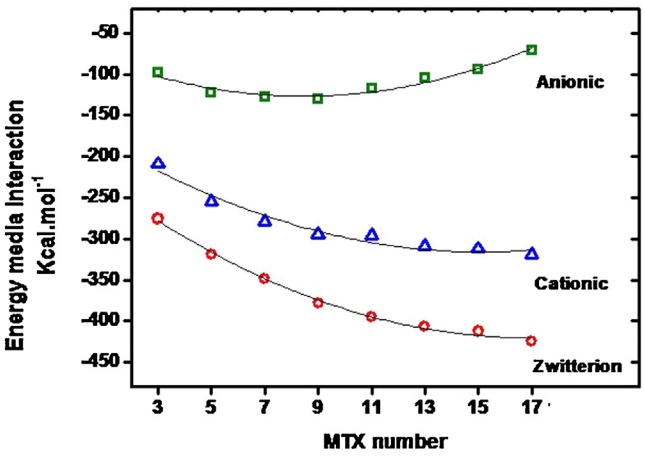

Fig. 5. Interaction energies of methotrexate (MTX) molecules in different charge states: anionic, zwitterionic and cationic.

Fig. 4 shows the clusters with different quantities of MTX molecules (3, 5, 7, 9, 11, and 17) in different charge states (anionic, zwitterionic and cationic). A weak interaction between MTX molecules was observed in the anionic state, whereas in the zwitterionic and cationic states, a strong interaction between MTX

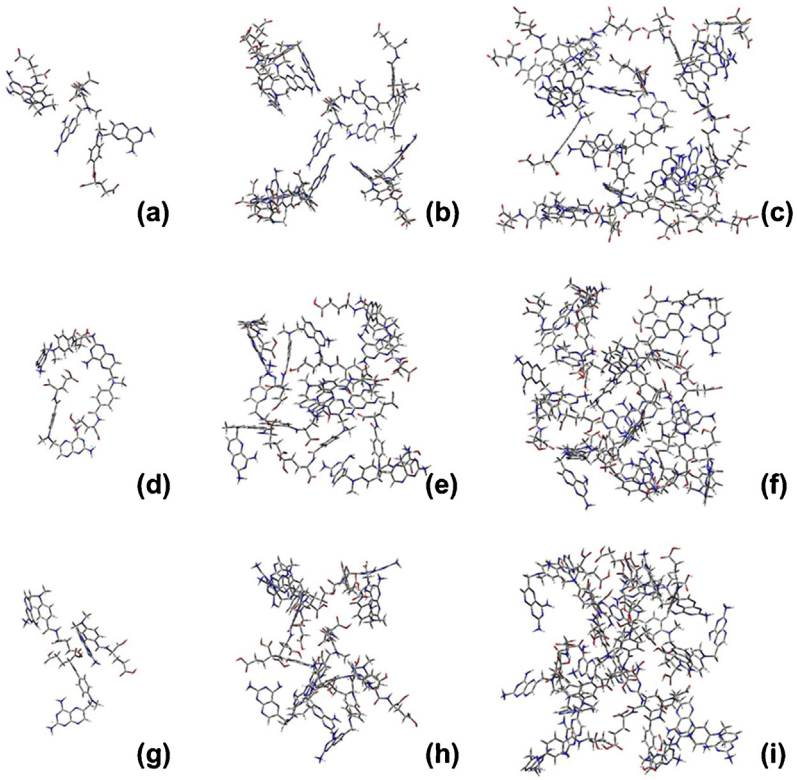

Fig. 4. Clusters with different quantities of methotrexate (MTX) molecules in different charge states: anionic (a–c), zwitterionic (d–f) and cationic (g–i).

molecules was observed. These results are shown in Fig. 5, which shows the relationships between the interaction energies of the MTX molecules. The anionic molecules presented an average energy of approximately −110 kcal/mol for clusters with up to nine molecules; as the number of molecules increased over nine, the energy also increased, which suggested a less favorable clustering state. However, the cationic and zwitterionic species displayed average interaction energies around −260 and −360 kcal/mol, respectively. This energy trend of increasingly negative values clearly indicated a more energetically favorable state for the formation of clusters. Therefore, from an energy stand point, MTX molecules in cationic and zwitterionic states were more likely to be aggregated.

The calculated volume for each size and state (cationic, zwitterionic and anionic) of MTX cluster is displayed in Table 2. The results indicated that the clusters in the zwitterionic and cationic states (acidic pH) had larger volumes, observed mainly from the 7 MTX molecules, and higher energies of interaction between MTX molecules than did the clusters in the anionic state. This favored the aggregation of molecules in the cationic and zwitterionic states. The clusters in the anionic state (neutral pH) exhibited the lowest energy of interaction and cluster volume, which indicated a region energetically favorable to the formation of nanoparticles, and corroborated with the results mentioned above.

3.2. Experimental study

3.2.1. Effect of acid-base neutralization in preparation of MTX nanosuspensions

MTX nanosuspensions were prepared by chemical precipitation using a bottom-up approach. MTX exists in different ionic forms depending on the pH of the solution (Fig. 6). It is soluble in alkaline solutions, whereas, in solutions below its pKa values of 4.7 and 3.36, its solubility decreases. Neutralizing a basic solution containing MTX causes a decrease in solubility, which induces the formation of the zwitterionic and cationic forms and causes precipitation.

The challenge of the bottom-up process is to determine the optimal conditions for MTX solubilization and precipitation in order to obtain an appropriate particle size reduction. For initial screening, different alkaline conditions were evaluated in which one or two MTX carboxyl groups were ionized, in order to determine the best NaOH proportion in which to dissolve the drug. Thereafter, different acidic conditions were tested to determine the most appropriate proportion of acid that would lead to the precipitation of the drug in nano-size ranged particles. During these steps, different acid and base proportions were tested as critical parameters to obtain nanosuspensions. The nanosuspensions were evaluated using measurements of particle size, PDI, zeta potential, and final pH. The results are shown in Table 3.

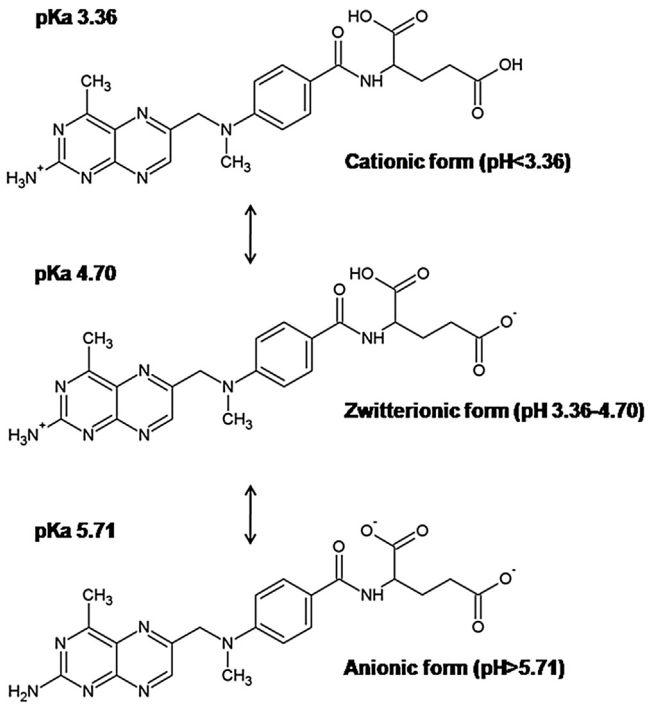

Fig. 6. Ionization of MTX.

Nanoparticles were formed for samples F1 (132 nm) and F2 (186 nm) (Table 3), using the lowest HCl proportion during the drug precipitation step. These formulations exhibited a homogeneous particle size distribution, as indicated by PDI values below 0.2 (Bose et al., 2012).

As the HCl proportion increased in the formulations F3, F4, F5, F6, F7, and F8, particle size and PDI values increased significantly. This was attributed to a high degree of supersaturation created by acid-base neutralization, which resulted in the formation of a large number of aggregated heterogeneous particles (Chen et al., 2004). Besides, the further addition of HCl led to a rapid growth of MTX cores, which aggregated into microparticles.

In the formulations with lower pHs, where microparticles or microsuspensions formed (F3, F4, F5, F6, F7 and F8), more study is necessary, including the evaluation of the use of stabilizers for preventing particle agglomeration and particle growth and the effect of other agitation processes on particle size reduction. These approaches represent promising strategies to be studied in the production of MTX nanosuspensions.

The zeta potential values were predominantly negative and increased as the pH of the samples increased. The negative zeta potential was attributed to the ionization of the carboxylic acid groups in the MTX molecule, which occurred at a pH above its pKa (=5.71) where the anionic form was predominant. Samples with an

Table 2
Calculated volumes for methotrexate (MTX) clusters in different charge states: anionic, zwitterionic, and cationic.

MTX molecules number	Cluster volume (Å^3)		
	Anionic	Zwitterion	Cationic
3	1143.17	1139.01	1163.51
5	1902.25	1896.66	1938.02
7	2661.80	2673.38	2717.48
9	3420.10	3433.68	3485.51
11	4179.86	4196.00	4259.00
13	4946.55	4972.19	5029.44
15	5700.65	5747.90	5810.76
17	6463.68	6512.97	6581.68

Table 3
Particle size, polydispersity index (PDI), zeta potential and final pH of methotrexate (MTX) nanosuspensions (mean ± SD, $n = 3$).

Sample	Particle size nm ± s.d.	PDI ± s.d.	Zeta potential mV ± s.d.	pH
F1[a]	132 ± 4.50	0.157 ± 0.01	−49.72 ± 0.30	6.36
F2[a]	186 ± 1.60	0.165 ± 0.17	−50.20 ± 0.10	6.08
F3[b]	3254 ± 356.00	0.674 ± 0.16	−43.88 ± 0.70	5.06
F4[b]	3927 ± 160.21	0.742 ± 0.05	−31.33 ± 0.15	4.01
F5[b]	5165 ± 436.37	0.841 ± 0.29	−17.30 ± 0.20	3.19
F6[c]	7308 ± 808.29	1.000 ± 0.00	−14.50 ± 1.73	2.65
F7[c]	2874 ± 148.91	0.583 ± 0.00	7.56 ± 1.39	1.38
F8[c]	6816 ± 243.43	1.000 ± 0.00	18.63 ± 1.03	1.16

a is anionic form, b is zwitterionic form and c is cationic form.

acidic pH (F7 and F8), on the other hand, exhibited positive zeta potentials because the amino group of MTX was protonated at a pH below its pKa (=3.36) where the cationic form was predominant. The zeta potential values indicated that, depending on the pH and the ionic form of the MTX, the surface charge of the particles varied from positive to negative. Higher zeta potential values were obtained for samples F1, F2, F3, and F4 and ranged from −31.33 to −50.20 mV. High values are desirable for promoting repulsion between particles with the same charge and for avoiding aggregation. Minimum zeta potential of ±30 mV is sufficient to stabilize nanosuspensions by electrostatic repulsion, and a zeta potential of approximately ±20 mV in combination with steric stabilization (Wang et al., 2013). Therefore, if the particles possessed sufficient zeta potential values to provide enough electric repulsion, particle aggregation was less likely to occur.

This study displayed the importance of determining the optimal precipitation conditions and how the conditions affect particle size. The different proportions of HCl influenced not only the particle size, but also the PDI, zeta potential values, and final pH of the MTX nanosuspensions. This study also indicated that it was possible to obtain nanosuspensions with a bottom-up method using acid-base neutralization reactions. In addition, the study provided guidance for controlling the size of the particles using different precipitation conditions.

3.2.2. Fourier transform infrared spectroscopy (FTIR)

The FTIR has been widely used to characterize interactions and/or structures of the drug at the molecular level, through change in the absorbance such as wavenumber or intensity which can be observed in the nanosuspensions and compared with the pure drug (Jog et al., 2016a).

FTIR spectra for MTX nanosuspensions (F2, F3, and F7) and raw MTX are shown in Fig. 7. The stretching vibration bands between 3400 cm^{-1} and 3300 cm^{-1} were due the appearance of broad peaks for the N—H and O—H groups (Chadha et al., 2009; Ekinci et al., 2015; Zhang et al., 2014) and the characteristic band at 1638 cm^{-1} corresponded to the presence of C=C stretching vibration (Ferreira et al., 2015; Lima and Reis, 2015). Similarly, vibration bands in the region of 1641 cm^{-1} indicated that C=O stretching partially overlapped the N—H band, which appeared around 1608 cm^{-1} (Ajmal et al., 2015; Chadha et al., 2009; Dai et al., 2015). Besides, the vibration band at 1208 cm^{-1} indicated C—N stretching (Chen et al., 2012; Tian et al., 2014; Zhang et al., 2014).

FTIR spectroscopy was performed to evaluate the molecular structure of the MTX particles after the bottom-up process followed by lyophilization. The comparisons between the spectra of raw MTX and those of MTX nanosuspensions demonstrated that there were no significant changes in the positions of the IR bands; however, there were slight variations in their intensities. These variations indicated that minor structural changes occurred at a molecular level, that is, the molecular spatial relationships of the MTX slightly changed after bottom-up processing. In this regard, disappearance or weakening of the absorption peaks corresponding to C=C, C=O, and N—H stretching were observed, especially in the spectra of F2. This may have resulted from its small particle size.

3.2.3. Attenuated total reflectance fourier transform infrared spectroscopy (ATR-FTIR)

The MTX nanosuspensions liquid form (F2, F3, and F7) and raw MTX were also analyzed using ATR-FTIR, and are shown in Fig. 8. A band intensity between 3700 cm^{-1} and 3100 cm^{-1} for nanosuspensions (F2, F3, and F7) was observed, which became more pronounced with presence of water, masking the broad bands for the N—H and O—H groups of the MTX between 3400 cm^{-1} and 3300 cm^{-1}. Moreover, the region between 3700 cm^{-1} and 3100 cm^{-1} corresponds to the O—H stretching vibrations, characteristic of the water molecule (Pirayavarapom et al., 2013).

It is important to notice that the vibration band at 1641 cm^{-1} indicated that C=O stretching overlapped the C=C stretching vibration band in 1638 cm^{-1}, as observed in the ATR-FTIR spectra F2, F3, and F7. Additionally, N—H vibration band in the region around 1608 cm^{-1}, and the vibration band at 1208 cm^{-1} corresponding to C—N stretching, demonstrated that the characteristic bands of the MTX continue evident for all liquid form nanosuspensions. However, a decrease in the bands intensity was observed, probably due the presence of water molecules.

These results demonstrated that there were no significant changes in the positions of the IR bands between spectra of the lyophilizated nanosuspensions and those liquid nanosuspensions, and these ATR-FTIR data are supportive for FTIR spectra of the solid nanosuspensions.

3.2.4. Drug content study

The MTX content for sample F7 was 99.84%, whereas, for F2, drug content was found to be 79.92%. This lowest drug content in the nanosuspension F2 can be attributed to the final pH (pH 6), at which the carboxyl group began to be ionized, which resulted in an increased quantity of MTX molecules outside of the

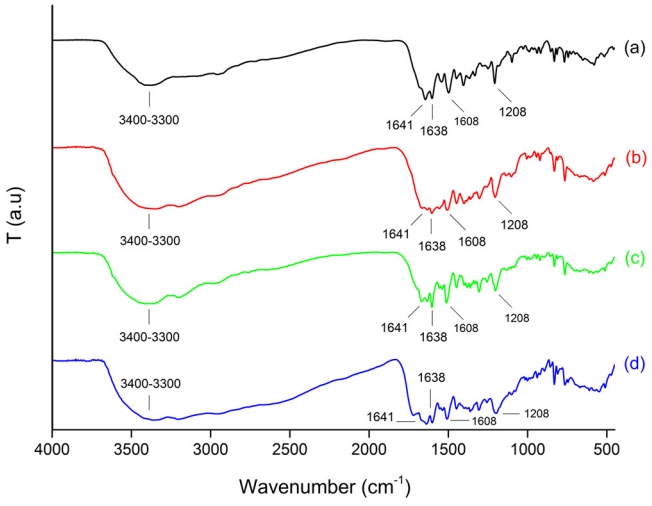

Fig. 7. FTIR spectra of: (a) raw methotrexate (MTX); (b) F2; (c) F3; and (d) F7.

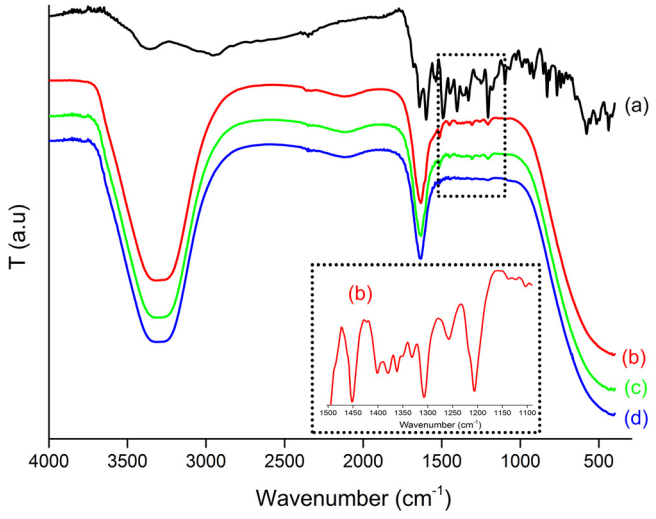

Fig. 8. ATR-FTIR spectra of: (a) raw methotrexate (MTX); (b) F2; (c) F3; and (d) F7.

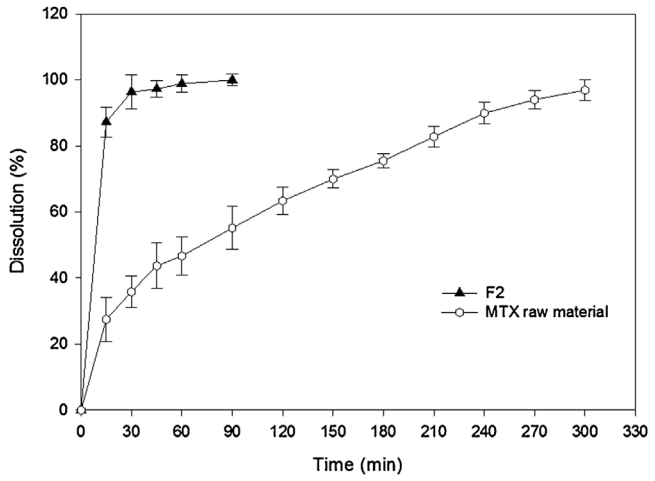

Fig. 9. Dissolution profiles of raw methotrexate (MTX) and F2 nanosuspension (composition in Table 1) in phosphate buffer (pH 6.8) as release medium.

nanosuspensions particles. Additionally, drug outside of the particles (in solution) may be an advantage if a burst effect is desired.

3.2.5. In vitro *dissolution of nanosuspensions*

Drug nanoparticles are one of the novel nano-medicine tools to overcome the problems of solubility and bioavailability of poorly water-soluble active pharmaceutical ingredients, through their combined mechanisms of enhancing dissolution rates and increasing supersaturation levels due to nano-size range (Jog et al., 2016b).

The dissolution profile of F2 was compared with that of raw MTX (Fig. 9). F2 displayed a higher rate of dissolution than raw MTX. F2 dissolved more than 80% of MTX in the first 15 min and 100% in less than 90 min. In contrast, raw MTX dissolved <30% of the drug in the first 15 min and took 300 min to dissolve the total amount. According to Chen et al. (2012), the size of the raw material can vary in the diameter, from 1 μm to over 5 μm. The increase in dissolution rate was attributed to particle sizes in the nano range, which presented greater surface areas according to the Noyes-Whitney equation (Noyes and Whitney, 1897) and a drug saturation solubility that followed the Ostwald-Freundlich equation (Li et al., 2011; Zhang et al., 2013).

From the *in vitro* dissolution results, it can be concluded that the nanosuspensions significantly increased the dissolution rate of MTX compared to that of the raw drug.

4. Conclusions

Molecular simulation using computational modeling indicated that MTX presented a favorable microaggregation trend. Despite of particle size reduction being a non favorable process from an energy view point, this study determined the experimental conditions required to obtain nanoparticles by controlling the molecular form of MTX (cationic, zwitterionic, or anionic) and the interactions between acids, bases and ionization groups on the MTX molecule.

The computational modeling corroborated the experimental results, in which microsuspensions were formed in samples with lower pH. This occurred because cationic forms of MTX were created that had decreased negative zeta potential, increased energy of interaction, and increased agglomeration. On the other hand, nanosuspensions were formed when the anionic form of MTX was predominant (neutral pH). The anionic form displayed a lower energy of interaction, resulting in smaller nano-ranged clusters. Thus, this study was essential for a comprehensive understanding of the development of MTX nanosuspensions based on computational modeling and acid-base neutralization, indicating that the computational methodologies were complementary to the experimental methodologies. These tools were crucial to the formation of nano-range size particles and to clarify that the parameters, including the ionic form of MTX, interaction energy, and drug precipitation, were directly related to the properties of these particles (size, PDI, zeta potential, and dissolution rate).

Acknowledgements

The financial support provided by CNPq (Conselho Nacional de Desenvolvimento Científico e Tecnológico), CAPES (Coordenação de Aperfeiçoamento de Pessoal de Nível Superior) "FAPESP (Fundação de Amparo a Pesquisa do Estado de São Paulo)", and FAPEMIG (Minas Gerais Research Foundation, grant # CDS APQ 00465/14) is acknowledged. We would like to acknowledge Dr. Bruno Leonardo Caetano of the Department of Drugs and Pharmaceuticals, Faculty of Pharmaceutical Sciences, São Paulo State University for their collaboration in this work.

References

Anon, 2017. Forcite, and Adsorption Locator Are Modules of Materials Studio Simulation Software Available from Accelrys. . http://accelrys.com/products/collaborative-science/biovia-materials-studio/.
Ajmal, M., Yunus, U., Matin, A., Haq, N.U., 2015. Synthesis, characterization and in vitro evaluation of methotrexate conjugated fluorescent carbon nanoparticles as drug delivery system for human lung cancer targeting. J. Photochem. Photobiol. B Biol. 153, 111–120.
Alaei, S., Ghasemian, E., Vatanara, A., 2016. Spray drying of cefixime nanosuspension to form stabilized and fast dissolving powder. Powder Technol. 288, 241–248.
Becke, A.D., 1988. Density-functional exchange-energy approximation with correct asymptotic behavior. Phys. Rev. A 38, 3098.
Bhavna, M.D.S., Ali, M., Ali, R., Bhatnagar, A., Baboota, S., Ali, J., 2014. Donepezil nanosuspension intended for nose to brain targeting: in vitro and in vivo safety evaluation. Int. J. Biol. Macromol. 67, 418–425.
Bose, S., Schenck, D., Ghosh, I., Hollywood, A., Maulit, E., Ruegger, C., 2012. Application of spray granulation for conversion of a nanosuspension into a dry powder form. Eur. J. Pharm Sci. 47, 35–43.
Bunker, A., Magarkar, A., Viitala, T., 2016. Rational design of liposomal drug delivery systems, a review: combined experimental and computational studies of lipid membranes, liposomes and their PEGylation. Biochim. Biophys. Acta Biomembr. 1858, 2334–2352 in press.
Chadha, R., Arora, P., Kaur, R., Saini, A., Singla, M., Jain, D., 2009. Characterization of solvatomorphs of methotrexate using thermoanalytical and other techniques. Acta Pharm. 59, 245–257.
Chen, J.F., Zhou, M.Y., Shao, L., Wang, Y.Y., Yun, J., Chew, N.Y.K., Chan, H.K., 2004. Feasibility of preparing nanodrugs by high-gravity reactive precipitation. Int. J. Pharm. 269, 267–274.
Chen, H., Wan, J., Wang, Y., Mou, D., Liu, H., Xu, H., Yang, X., 2008. A facile nanoaggregation strategy for oral delivery of hydrophobic drugs by utilizing acid-base neutralization reactions. Nanotechnology 19, 1–7.
Chen, A.Z., Li, L., Wang, S.B., Zhao, C., Liu, Y.G., Wang, G.Y., Zhao, Z., 2012. Nanonization of methotrexate by solution-enhanced dispersion by supercritical CO_2. J. Supercrit. Fluids 67, 7–13.
Collnot, E.M., Ali, H., Lehr, C.M., 2012. Nano- and microparticulate drug carriers for targeting of the inflamed intestinal mucosa. J. Control. Release 161, 235–246.
Dai, C.F., Li, S.P., Li, X.D., 2015. Synthesis of nanostructured methotrexate/hydroxyapatite: morphology control, growth mechanism, and bioassay explore. Colloids Surf. B 136, 262–271.
Das, S., Suresh, P.K., 2011. Nanosuspension: a new vehicle for the improvement of the delivery of drugs to the ocular surface. Application to amphotericin B. Nanomedicine 7, 242–247.
De Souza, L.A., Nogueira, C.A.S., Ortega, P.F.R., Lopes, J.F., Calado, H.D.R., Lavall, R.L., Silva, G.G., Dos Santos, H.F., De Almeida, W.B., 2016. Inclusion complex between cisplatin and single-walled carbon nanotube: an integrated experimental and theoretical approach. Inorg. Chim. Acta 447, 38–44.
Dennington, R., Keith, T., Millam, J., 2009. GaussView Version 5. Semichem, Inc., Shawnee Mission, KS.
Ekinci, M., Ilem-Ozdemir, D., Gundogdu, E., Asikoglu, M., 2015. Methotrexate loaded chitosan nanoparticles: preparation, radiolabeling and in vitro evaluation for breast cancer diagnosis. J. Drug Deliv. Sci. Technol. 30, 107–113.

Ferreira, M., Chaves, L.L., Lima, S.A.C., Reis, S., 2015. Optimization of nanostructured lipid carriers loaded with methotrexate: a tool for inflammatory and cancer therapy. Int. J. Pharm. 492, 65–72.
Frisch, M.J., Trucks, G.W., Schlegel, H.B., Scuseria, G.E., Robb, M.A., Cheeseman, J.R., Scalmani, G., Barone, V., Mennucci, B., Petersson, G.A., Nakatsuji, H., Caricato, M., Li, X., Hratchian, H.P., Izmaylov, A.F., Bloino, J., Zheng, G., Sonnenberg, J.L., Hada, M., Ehara, M., Toyota, K., Fukuda, R., Hasegawa, J., Ishida, M., Nakajima, T., Honda, Y., Kitao, O., Nakai, H., Vreven, T., Montgomery Jr, J.A., Peralta, J.E., Ogliaro, F., Bearpark, M., Heyd, J.J., Brothers, E., Kudin, K.N., Staroverov, V.N., Kobayashi, R., Normand, J., Raghavachari, K., Rendell, A., Burant, J.C., Iyengar, S.S., Tomasi, J., Cossi, M., Rega, N., Millam, J.M., Klene, M., Knox, J.E., Cross, J.B., Bakken, V., Adamo, C., Jaramillo, J., Gomperts, R., Stratmann, R.E., Yazyev, O., Austin, A.J., Cammi, R., Pomelli, C., Ochterski, J.W., Martin, R.L., Morokuma, K., Zakrzewski, V. G., Voth, G.A., Salvador, P., Dannenberg, J.J., Dapprich, S., Daniels, A.D., Farkas, Ö., Foresman, J.B., Ortiz, J.V., Cioslowski, J., Fox, D.J., 2009. Gaussian 09. Gaussian Inc, Wallingford CT.
Gece, G., 2008. The use of quantum chemical methods in corrosion inhibitor studies. Corros. Sci. 50, 2981–2992.
George, M., Ghosh, I., 2013. Identifying the correlation between drug/stabilizer properties and critical quality attributes (CQAs) of nanosuspension formulation prepared by wet media milling tecnology. Eur. J. Pharm. Sci. 48, 142–152.
Hansch, C., Leo, A., Hoekman, D.H., 1995. Exploring QSAR – hydrophobic, electronic, and steric constants. Am. Chem. Soc. Washington, USA (pp. 1071).
Jacobs, C., Müller, R.H., 2002. Production and characterization of a budesonide nanosuspension for pulmonary administration. Pharm. Res. 19, 189–194.
Jog, R., Gokhale, R., Burgess, D.J., 2016a. Solid state drug-polymer miscibility studies using the model drug ABT-102. Int. J. Pharm. 509, 285–295.
Jog, R., Kumar, S., Shen, J., Jugade, N., Tan, D.C.T., Gokhale, R., Burgess, D.J., 2016b. Formulation design and evaluation of amorphous ABT-102 nanoparticles. Int. J. Pharm. 498, 153–169.
Kokalj, A., Peljhan, S., 2010. Density functional theory study of ATA, BTAH, and BTAOH as copper corrosion inhibitors: adsorption onto Cu(111) from gas phase. Langmuir 26, 14582–14593.
Lewars, E.G., 2003. Computational Chemistry: Introduction to the Theory and Applications of Molecular and Quantum Mechanics. Kluwer Academic Publishers, Norwell, USA.
Li, W., Yang, Y., Tian, Y., Xu, X., Chen, Y., Mu, L., Zhang, Y., Fang, L., 2011. Preparation and *in vitro/in vivo* evaluation of revaprazan hydrochloride nanosuspension. Int. J. Pharm. 408, 157–162.
Li, L., Cai, T., Wang, Z., Zhou, Z., Geng, Y., Sun, T., 2014. Study on molecular structure, spectroscopic investigation (IR, Raman and NMR), vibrational assignments and HOMO-LUMO analysis of L-sodium folinate using DFT: a combined experimental and quantum chemical approach. Spectrochim. Acta A 120, 106–118.
Lima, S.A.C., Reis, S., 2015. Temperature-responsive polymeric nanospheres containing methotrexate and gold nanoparticles: a multi-drug system for theranostic in rheumatoid arthritis. Colloids Surf. B 133, 378–387.
Möschwitzer, J.P., 2013. Drug nanocrystals in the commercial pharmaceutical development process. Int. J. Pharm. 453, 142–156.
Macedo, M.C.S.S., Barcia, O.E., Da Silva, E.C., Mendes, J., De, O., Mattos, O.R., 2012. Iron corrosion inhibition by Imidazole in 3.5% NaCl medium: experimental and theoretical results. J. Electrochem. Soc. 159, 160–169.
Mou, D., Chen, H., Wan, J., Xu, H., Yang, X., 2011. Potent dried drug nanosuspensions for oral bioavailability enhancement of poorly soluble drugs with pH-dependent solubility. Int. J. Pharm. 413, 237–244.
Noyes, A.A., Whitney, W.R., 1897. The rate of solution of solid substances in their own solutions. J. Am. Chem. Soc. 19, 930–934.
Pereira, A.F., Costa, V.M., Santos, M.C.M., Pinto, F.C.H., Silva, G.R., 2014. Evaluation of the effects of methotrexate released from polymeric implants in solid Ehrlich tumor. Biomed. Pharmacother. 68, 365–368.
Pignatello, R., Bucolo, C., Spedalieri, G., Maltese, A., Puglisi, G., 2002. Flurbiprofen-loaded acrylate polymer nanosuspensions for ophthalmic application. Biomaterials 23, 3247–3255.
Pirayavarapom, C., Rades, T., Gordon, K.C., Tucker, I.G., 2013. Quantification of the types of water in Eudragit RLPO polymer and the kinetics of water loss using FTIR. Int. J. Pharm. 458, 90–98.
Rabinow, B.E., 2004. Nanosuspensions in drug delivery. Nat. Rev. Drug Discov. 3, 785–796.
Ramezanpour, M., Leung, S.S.W., Delgado-Magnero, K.H., Bashe, B.Y.M., Thewalt, J., Tieleman, D.P., 2016. Computational and experimental approaches for investigating nanoparticle-based drug delivery systems. Biochim. Biophys. Acta Biomembr. 1858, 1688–1709.
Rappe, A.K., Casewit, C.J., Colwell, K.S., Goddardlll, W.A., Skiff, W.M., 1992. UFF, a full periodic table force field for molecular mechanics and molecular dynamics simulations. J. Am. Chem. Soc. 114, 10024–10035.
Rappe, A.K., Colwell, K.S., Casewit, C.J., 1993. Application of a universal force field to metal complexes. Inorg. Chem. 32, 3438–3450.
Rassolov, V.A., Ratner, M.A., Pople, J.A., Redfern, P.C., Curtiss, L.A., 2001. 6-31G* basis set for third-row atoms. J. Comp. Chem. 22, 976–984.
Rubino, F.M., 2001. Separation methods for methotrexate, its structural analogues and metabolites. J. Chromatogr. B Biomed. Sci. Appl. 764, 217–254.
Sinha, B., Müller, R.H., Möschwitzer, J.P., 2013. Bottom-up approaches for preparing drug nanocrystals: formulations and factors affecting particle size. Int. J. Pharm. 453, 126–141.
Tian, X., Li, H., Zhang, D., Shen, J., Jia, L., Zheng, D., Liu, G., Hao, L., Shen, Y., Zhang, Q., 2013. Parenteral nanosuspension of a novel synthesized antitumor candidate: investigation of tissue biodistributions and plasma pharmacokinetics. Colloids Surf. A 436, 868–872.
Tian, D.Y., Liu, Z.L., Li, S.P., Li, X.D., 2014. Facile synthesis of methotrexate intercalated layered double hydroxides: particle control, structure and bioassay explore. Mater. Sci. Eng. C 45, 297–305.
Tomasi, J., Mennucci, B., Cammi, Roberto, 2005. Quantum mechanical continuum solvation models. Chem. Rev. 105, 2999–3093.
United States Pharmacopeia & National Formulary, 30th ed. Rockville: United States Pharmacopeial Convention, Easton: Mack, 2007.
Verma, S., Gokhale, R., Burgess, D.J., 2009. A comparative study of top-down and bottom-up approaches for the preparation of micro/nanosuspensions. Int. J. Pharm. 380, 216–222.
Wang, Y., Zheng, Y., Zhang, L., Wang, Q., Zhang, D., 2013. Stability of nanosuspensions in drug delivery. J. Control. Release 172, 1126–1141.
Xu, Y., Liu, X., Lian, R., Zheng, S., Yin, Z., Lu, Y., Wu, W., 2012. Enhanced dissolution and oral bioavailability of aripiprazole nanosuspensions prepared by nanoprecipitation/homogenization based on acid-base neutralization. Int. J. Pharm. 438, 287–295.
Zhang, K., Yu, H., Luo, Q., Yang, S., Lin, X., Zhang, Y., Tian, B., Tang, X., 2013. Increased dissolution and oral absorption of itraconazole/soluplus extrudate compared with itraconazole nanosuspension. Int. J. Pharm. Biopharm. 85, 1285–1292.
Zhang, X.Q., Zeng, M.G., Li, S.P., Li, X.D., 2014. Methotrexate intercalated layered double hydroxides with different particle sizes: structural study and controlled release properties. Colloids Surf. B 117, 98–106.